Plant Science 238 (2015) 286–296

Contents lists available at ScienceDirect

Plant Science

journal homepage: www.elsevier.com/locate/plantsci

K^+ accumulation in the cytoplasm and nucleus of the salt gland cells of *Limonium bicolor* accompanies increased rates of salt secretion under NaCl treatment using NanoSIMS

Zhong-Tao Feng[a,1], Yun-Quan Deng[a,1], Shi-Chao Zhang[a], Xue Liang[a], Fang Yuan[a], Jia-Long Hao[b], Jian-Chao Zhang[b], Shu-Feng Sun[c,d], Bao-Shan Wang[a,*]

[a] Key Laboratory of Plant Stress Research, College of Life Science, Shandong Normal University, Jinan 250014, China
[b] Key Laboratory of the Earth's Deep Interior, Institute of Geology and Geophysics, Chinese Academy of Sciences, Beijing 100029, China
[c] National Laboratory of Biomacromolecules, Institute of Biophysics, Chinese Academy of Sciences, Beijing 100101, China
[d] Center for Bio-Imaging, Institute of Biophysics, Chinese Academy of Sciences, Beijing 100101, China

ARTICLE INFO

Article history:
Received 21 April 2015
Received in revised form 17 June 2015
Accepted 22 June 2015
Available online 26 June 2015

Keywords:
Elemental localization
Limonium bicolor
NanoSIMS
NMT
Salt gland
Ultrastructure

ABSTRACT

Recretohalophytes with specialized salt-secreting structures (salt glands) can secrete excess salts from plant, while discriminating between Na^+ and K^+. K^+/Na^+ ratio plays an important role in plant salt tolerance, but the distribution and role of K^+ in the salt gland cells is poorly understood. In this article, the *in situ* subcellular localization of K and Na in the salt gland of the recretohalophyte *Limonium bicolor* Kuntze is described. Samples were prepared by high-pressure freezing (HPF), freeze substitution (FS) and analyzed using NanoSIMS. The salt gland of *L. bicolor* consists of sixteen cells. Higher signal strength of Na^+ was located in the apoplast of salt gland cells. Compared with control, 200 mM NaCl treatment led to higher signal strength of K^+ and Na^+ in both cytoplasm and nucleus of salt gland cells although K^+/Na^+ ratio in both cytoplasm and nucleus were slightly reduced by NaCl. Moreover, the rate of Na^+ secretion per salt gland of *L. bicolor* treated with 200 mM NaCl was five times that of controls. These results suggest that K^+ accumulation both in the cytoplasm and nucleus of salt gland cells under salinity may play an important role in salt secretion, although the exact mechanism is unknown.

1. Introduction

Soil salinization is a major problem worldwide, with more than 950 million hectares of land being salt-affected. Soil salinity severely reduces agricultural yields and productivity [1]. Salinity may cause a decrease in biomass production due to a lowering of plant water potentials, and/or specific ion toxicities [2]. Uptake of a high concentration of Na^+ into cells damages plasma membranes and leads to an imbalance of ions including a loss of Ca^{2+} and K^+, metabolic disorder, and reduced plant growth [3,4]. Salt tolerance depends to a great extent on the location of ions and especially of Na^+, K^+, and Cl^-. So, the capacity of plants to maintain sufficient K^+ may be an important factor providing a degree of salt tolerance in plants [5]. Salt-tolerant plants can reduce injury from salt stress by decreasing their cellular Na^+ and increasing their cellular K^+ concentrations to maintain a favorable K^+/Na^+ ratio, which is critical in plant salinity tolerance [1]. Low Na^+ and high K^+ in the cytoplasm are essential for the maintenance of a number of enzymatic processes and protein synthesis [6]. The capacity of plants to counteract salinity stress will strongly depend on the status of their K^+ nutrition [7]. K^+ is an indispensable macronutrient and the most abundant cation in most plants, whose functions can roughly be summarized as (i) charge balancing in the cytoplasm, where K^+ is the dominant counterion for the large excess of negative charge on proteins and nucleic acids; (ii) activation of crucial enzymatic reactions; (iii) and making a substantial contribution to the osmotic pressure of the vacuole. In contrast, Na^+ is only essential for a

Abbreviations: DAPI, 4′,6-diamidino-2-phenylindole; DM, dry mass; FS, freeze substitution; HPF, high-pressure freezing; LSCM, laser scanning confocal microscope; MRP, mass resolving power; NMT, non-invasive micro-test technology; PPFD, photosynthetic photon flux density; SE, secondary electron; SEM, scanning electron microscope; SIMS, secondary ion mass spectrometry; TEM, transmission electron microscope.

* Corresponding author. Fax: +86 53186180107.
E-mail addresses: ztfeng305@126.com (Z.-T. Feng), bayu18@163.com (Y.-Q. Deng), zsc2012sdnu@163.com (S.-C. Zhang), qingshuiyu1223@qq.com (X. Liang), yuanfang19861114@126.com (F. Yuan), sean_hao@mail.iggcas.ac.cn (J.-L. Hao), zhangjc850206@126.com (J.-C. Zhang), ssf@moon.ibp.ac.cn (S.-F. Sun), bswang@sdnu.edu.cn (B.-S. Wang).
[1] These authors contributed equally to this work.

http://dx.doi.org/10.1016/j.plantsci.2015.06.021
0168-9452/

number of C_4 or crassulacean acid metabolism (CAM) photosynthesis species, where it functions as a micronutrient. In all other species Na^+ does not act as a nutrient because it is not required for normal plant growth [7–9].

According to their salinity resistance, plants can be divided into halophytes and glycophytes. Halophytes, plants that can survive to reproduce in an environment where the salt (NaCl) concentration is around 200 mM or more, are further divided into recretohalophytes, euhalophytes, and pseudo-halophytes based on their physiological mechanism of salinity tolerance, morphologic structures, and ecological characteristics [10,11]. The most remarkable features of recretohalophytes are the specialized salt-secreting structures including salt glands and salt bladders that can secrete or sequestrate excess salts out of cells of the main body of the leaf. A salt gland is an excretory organ that plays a prominent role in regulating ion balance, maintaining the stability of osmotic pressure, and enhancing the salinity tolerance of plants under salinity [12]. With the spread of soil salinization worldwide, it has become increasingly important to understand the salt-tolerance mechanisms of halophytes. Transmission electron microscope (TEM) provides the resolution necessary to show precise details of such glands and has contributed significantly to our understanding of their ultrastructure in recretohalophytes [13,14]. In the last century, TEM combined with X-ray microanalysis has been widely used to elucidate the ultrastructure and localize the ions in the salt gland cells [15], and three hypotheses for the secretory mechanism of salt glands have been proposed. Arisz et al. [16] argued that salt secretion was a consequence of pressure generated in the gland cells; Ziegler and Lüttge [17] and Shimony and Fahn [18] proposed that salt secretion involved exocytosis; Levering and Thomson [14] suggested that salt secretion was similar to animal transport systems, but up to now, none of these hypotheses has been verified [12]. The main experimental obstacle to elucidating the mechanism of secretion is ion movement between cytoplasm and organelles during TEM sample preparation [19]. Another restriction is that X-ray microanalysis lacks the sensitivity to detect most mineral nutrients at physiological concentrations in plant tissues and needs further improvement on the collection efficiency of the X-ray detectors [20]. Consequently, the function of K^+ in salt gland cells in determining the salt tolerance of recretohalophytes is poorly understood. Most previous work has only considered the whole tissue K^+ concentration and our understanding of the importance of K^+ within the salt gland cells is limited. To evaluate this, more direct evidence is required using new methods of both sample preparation and elemental localization at the subcellular level.

Producing an accurate and nanoscale resolution image of the distribution of elements at the subcellular level is one of the greatest challenges in biology. Research on ion transport phenomena in plant cells has become increasingly dependent on the techniques that yield information about the subcellular localization of elements [21,22]. Likewise, knowledge of the distribution and concentration of ions within cells is an essential part of understanding their role in salt tolerance [23]. However, available data in previous studies has been limited by the compromises between resolution and sensitivity. If the distribution and localization of elements *in situ* can be visually mapped at the subcellular level, it will provide a new insight into salt excretion in recretohalophytes and the role of the key chemical elements such as K^+ in determining salt tolerance. Such information will also provide important clues to understanding the mechanisms of ion uptake, transport and secretion of salt gland cells.

Specimen preparation methodologies based on high-pressure freezing (HPF) and freeze substitution (FS) have made great progresses in the quality of ultrastructural preservation of biological samples for electron microscopy observation [24]. HPF uses liquid nitrogen applied at 210 MPa (2048 bar) to preserve biological samples in a 'close-to-native' state by freezing to vitreous ice generally with a depth of 200 μm. Also, HPF can immobilize the constituents of cells, arrest vital processes, and minimize the redistribution of diffusible substances such as Na^+ and K^+ [25]. After HPF, FS is a good choice to maintain the structure and constituents by removing the vitreous ice and fixing the ultrastructure of the sample at a temperature from −90 °C to 0 °C [26]. Thus, HPF followed by FS has become the standard protocol of choice for preserving plant tissues for studying ultrastructural details with TEM [22,27].

Secondary ion mass spectrometry (SIMS) microscopy is a secondary ion imaging technique that uses an energetic primary ion beam to remove particles from the uppermost few atomic layers of the biological specimen surface. The ions emitted during this bombardment known as secondary ions, are analyzed in a mass spectrometer to provide chemical information about the elemental distribution of the sample [28–30]. Technically speaking, the NanoSIMS is a dynamic, double-focussing, magnetic-sector, multi-collection capability scanning ion microprobe [31,32]. The NanoSIMS secondary ions are produced by bombardment of the sample with either O^- for electropositive ions or Cs^+ to generate negative ions. Use of the Cs^+ source has an added advantage that the secondary electron (SE) image can also be detected, allowing the sample surface topography and morphology to be imaged [33,34]. NanoSIMS is characterized by three fundamental characteristics: (i) high spatial resolution down to 50 nm for Cs^+ primary ions and 150 nm for O^- primary ions, so elemental imaging is at the nanoscale; (ii) high sensitivity and specificity for the secondary ion, detecting very low elemental concentration; and (iii) high mass resolution, which can be 22 times between minimum mass and maximum mass, so the instrument is able to detect most elements in the periodic table, from hydrogen to uranium, as well as their different isotopes [35,36]. These characteristics offer many advantages for the analysis of elemental distributions in plant cells at the cellular and, crucially, subcellular level. NanoSIMS has been applied to plants in a number of studies particularly those trying to resolve the distribution of chemical elements in the central vacuole, cytoplasm, and cell wall, for which the high resolution is required [37–40].

NanoSIMS analysis must be conducted under an ultra-high vacuum, meaning that complicated sample preparation protocols must be used in order to preserve the *in vivo* distribution of diffusible elements and morphology. So, biological samples should be preserved to a 'close-to-native' state so that their constituents are conserved when the sample preparation is completed [32]. Nowadays, it is generally accepted that HPF followed by FS is the preferred strategy [22,41,42]. Recent study using the combination of the HPF, FS, and NanoSIMS analysis, the homogeneous distribution of nickel was observed in the vacuole, notably in epidermal cells [22,43,44], which provided us the new idea on ions location analysis in plant excretory organs. In this article, we report ultrastructural features of the salt gland of *Limonium bicolor*, a typical recretohalophyte, which has been widely researched in the past [45–48], and the distribution of K and Na at their natural locations in the salt gland cells using the combination of HPF and FS with NanoSIMS to provide an insight into the function of K^+ in the cells of salt glands in determining the salt tolerance of recretohalophytes.

2. Materials and methods

2.1. Plant materials and growth conditions

L. bicolor Kuntze (Plumbaginaceae) seeds were collected from native saline-alkaline soil (N37°20′, E118°36′) in the Yellow River Delta, China. Dry seeds were stored in a refrigerator at <4 °C before being used. The seeds were surface disinfected in

0.1% (w/v) $HgCl_2$ for 10 min and then thoroughly washed with deionized water. Fully filled seeds were selected and planted in plastic pots (22 cm high × 20 cm diameter) filled with river sand that had been thoroughly rinsed with deionized water. After germination, the seedlings were grown in a controlled greenhouse (15 h photoperiod; 600 μmol m^{-2} s^{-1} light intensity; PPFD was 500 μmol m^{-2} s^{-1}; 30 ± 3 °C in the day and 20 ± 2 °C at night; 70% ± 10% relative humidity) and irrigated every day, until they reached the sixth-leaf stage, with full-strength Hoagland nutrient solution (pH adjusted to 5.7 ± 0.1 with NaOH and HCl and with the following composition: 2.5 mM $Ca(NO_3)_2$, 2.5 mM KNO_3, 1 mM $MgSO_4$, 0.5 mM KH_2PO_4, 45 μM Fe-EDTA, 23 μM H_3BO_3, 4.55 μM $MnCl_2$, 0.16 μM $CuSO_4$, 0.38 μM $ZnSO_4$, 0.28 μM Na_2MoO_4).

2.2. Treatments

Following emergence of the sixth leaf (from the shoot base), uniform and vigorous seedlings were selected and transferred into plastic pots (22 cm high × 20 cm diameter) containing well-washed river sand (three plants per pot). Control plants were irrigated with full-strength Hoagland nutrient solution (0 mM NaCl) while others were treated with 200 mM NaCl. The NaCl was dissolved in the nutrient solution described above. To avoid osmotic shock, the NaCl concentration was stepped up by 50 mM per day until the final concentration (200 mM) was achieved. To avoid salt accumulation in the sand due to evaporation, each pot was flushed with 2000 ml nutrient solution containing the respective concentrations of NaCl twice daily and allowed to drain. The experiment was terminated 28 d after the final salinity concentrations had been reached and the fully expanded sixth leaf from each plant was harvested for experiments. Five replicate pots were used for each treatment.

2.3. TEM observation

Healthy leaves of *L. bicolor* were selected and tissue segments (1.5 mm diameter and 200 μm thick) were dissected from each leaf. Each segment was placed in a 3 mm diameter copper carrier, which was filled with hexadecene. The carrier with the sample was immediately frozen using a Leica EM PACT2 high-pressure freezer, which subjected the sample to a pressure of 210 MPa at −196 °C for 30 ms.

FS with acetone was carried out in a Leica EM AFS2 system. The carriers with specimens were placed in 1.5 ml vials containing the substitution medium, 2% (w/v) osmium tetroxide in acetone, which had been previously frozen in liquid nitrogen. The vials with specimens were then transferred into the FS unit pre-cooled to −140 °C.

The FS system was programmed as follows. The temperature in the chamber was raised to −90 °C within 30 min then maintained at −90 °C for 84 h, after which it was raised at a rate of 5 °C per hour to −60 °C then maintained at −60 °C for 24 h. The temperature was then raised at a rate of 5 °C per hour to −30 °C and maintained at −30 °C for 24 h. This was followed by further raising the temperature to 0 °C, at a rate of 5 °C per hour, and maintaining it at 0 °C for 4 h. At this stage the acetone substitution medium was replaced with anhydrous acetone. On completion, samples were removed from the FS machine and placed at room temperature. All subsequent steps were carried out at room temperature (20 °C). Samples were rinsed with anhydrous acetone three times, each time for 20 min. Samples were then carefully removed from the carriers and embedded gradually in Spurr resin without accelerator. A graded resin/acetone (v/v) series was used: 10%, 25%, 50%, 75%, and 100% resin, with each step lasting 2 h. Samples were then placed in 100% resin without accelerator for 8 h and in 100% resin with accelerator for 8 h; this step was repeated five times. Samples were then placed in molds containing fresh resin and were polymerized for 9 h at 70 °C [22,33].

Sections of 70 nm thickness were cut and mounted onto copper grids coated with formvar for TEM analysis. Samples were stained in 1% (w/v) uranyl acetate in ethanol for 15 min and in lead citrate for a further 5 min. Micrographs were obtained with a FEI TECNAI20 TEM at 120 kV using a Gatan UltraScan 1000CCD camera.

2.4. NanoSIMS analysis

Sections of 500 nm thickness were also cut using a diamond knife on a Leica EM UC6 Ultramicrotome and mounted on solid silicium substrate. The samples were then coated with carbon to increase their conductivity for NanoSIMS analysis. The secondary ion maps were acquired by the CAMECA NanoSIMS 50 L at the Institute of Geology and Geophysics, Chinese Academy of Sciences. The CAMECA NanoSIMS 50 L used for this study was the latest generation of dynamic SIMS instrument, optimizing SIMS analysis performance [49]. The instrument was calibrated using standard calibration samples of silicon patterned with square mesas. Firstly, in order to obtain high resolution images of the leaf sections, a high intensity Cs^+ primary beam was used to remove surface contamination and implant the primary ions. Then using a low intensity primary Cs^+ ion beam for scanning the salt gland (the beam size was ~100 nm, the current was ~1–1.5 pA). Secondary ions were sputtered from the sample surface and detected simultaneously (in multi-collection mode) with the high mass resolving power (MRP) tuned to ~6000 ($M/\Delta M$, CAMECA definition). We used Nist 610 (K concentration is ~400 ppm) as our standard to check the correct position of the $^{39}K^{16}O^-$. As well as the $^{39}K^{16}O^-$ signal, we also selected the $^{16}O^-$ and $^{12}C^{14}N^-$ signals by rastering a 30 × 30 μm^2 areas in 51 × 512 pixels and 10 ms/pixel dwell time to assist in interpreting the distribution of elements between different subcellular compartments. The image capture took approximately 1 h. A primary O^- ion beam (the beam size was ~300 nm, the current was ~15–20 pA) was used to scan the salt gland for positive ions (Na^+). The other imaging conditions used were the same as for the Cs^+ primary beam. NanoSIMS data were analyzed using ImageJ with the OpenMIMS plugin (Harvard, Cambridge, MA, USA).

2.5. Fluorescence microscope observation

Fluorescence microscopy was performed according to the method of Nagata et al. [50]. Thin sections of *L. bicolor* leaves embedded in Technovit 7100 resin were stained with 4′,6-diamidino-2-phenylindole (DAPI) and examined under an Olympus BHS–RFK fluorescence microscope (Tokyo). In brief, healthy leaves of *L. bicolor* were fixed in 3% glutaraldehyde dissolved in 100 mM sodium cacodylate buffer (pH 7.4) for at least 24 h at 4 °C, dehydrated through an ethanol series, and then embedded in Technovit 7100 resin (Kulzer and Company, Wehrheim, Germany). The samples were sectioned (500 nm thick) with a glass knife on an Ultracut microtome (Leica, Wien, Austria) and dried on cover slips. Next, they were stained with 1 μg ml^{-1} DAPI in TAN buffer (20 mM Tris–HCl, pH 7.6, 0.5 mM EDTA, 7 mM β-mercaptoethanol, 1.2 mM spermidine). To prevent fading, 1 mg ml^{-1} *n*-propyl gallate in 50% glycerol was added to the samples before examination in the fluorescence microscopic. Photomicrographs of the samples were captured with a cooled CCD camera (Spot-RT; Diagnostic Instruments, Sterling Heights, MI) attached to the microscope [51].

2.6. Determination of leaf inorganic ions concentration

The fully expanded sixth leaves of *L. bicolor* under NaCl concentration treatments (0, or 200 mM) were harvested separately. After the leaves were thoroughly rinsed with distilled water to remove from the surface all salt that had been secreted previously, they were heated at 105 °C for 15 min to deactivate enzyme activity,

and then dried at 80 °C to a constant dry mass (DM). A 50 mg dry sample was ashed in a muffle stove at 550 °C for 2 d and the ash was dissolved in 1 ml of concentrated nitric acid. After the volume was increased to 25 ml with deionized water, the solution was filtered and the cations (Na^+ and K^+) were analyzed by the Dionex ICS-1100 ion chromatography system (Dionex Corp., Sunnyvale, CA, USA).

2.7. Determination of ions secretion rate in leaf discs

Fully expanded sixth leaves from plants grown in NaCl concentrations of 0, or 200 mM were thoroughly rinsed with distilled water to remove from the surface all salt that had been secreted previously, and 10-mm-diameter discs were punched from the leaves. The discs were dried quickly on both sides using absorbent paper then placed in 70 mm diameter Petri dishes containing 30 ml deionized water, abaxial surface uppermost. The abaxial leaf disc surface was covered with mineral oil (Sigma, M8410) to allow volumetric analyses of the secretion fluids [52–54]. With time, secretory droplets appeared under the oil above the salt glands and were collected with a micropipette. The experiment was conducted over a 24 h period at room temperature (20 °C) with a 12 h photoperiod. The volume of secretory droplets (V) per leaf disc was determined and their ionic concentration (C) measured by the Dionex ICS-1100 ion chromatography system (Dionex Corp., Sunnyvale, CA, USA). The ion secretion rate (pmol gland^{-1} h^{-1}) was calculated as [$V \times C$/(number of salt gland per leaf disc × time)] where number of salt gland per leaf disc was calculated as density of salt gland (number cm^{-2}) × area of leaf disc (cm^2) and time was duration of the secretion (from covering with mineral oil to collecting the droplets: hours).

2.8. Preparation for abaxial epidermal peels

The fully expanded sixth leaves from treated (0, or 200 mM NaCl) plants were washed five times with distilled water to remove ions from the surface and dried quickly on both sides using absorbent paper. Next, leaves were cut into 2 cm squares and transferred with the abaxial surface facing up to a small Petri dish (70 mm diameter) filled with buffer solution (0.1 mM NaCl, 0.1 mM KCl, 0.15 mM $CaCl_2$, and 0.3 mM MES, pH 6.0). To separate the abaxial epidermis, a pair of sharp forceps was used to fix each peel in the buffer and another pair of sharp forceps was used to split the abaxial epidermis from the leaf edge. The ions fluxes were measured from salt glands, as described below.

2.9. Selective ion flux measurements

Net fluxes of Na^+ and K^+ were measured non-invasively in YoungerUSA (Xuyue, Beijing, China) NMT (non-invasive micro-test technology) Service Center using a non-invasive micro-test technique (NMT-YG-100, YoungerUSA LLC, Amherst, MA01002, USA) with ASET 2.0 (Sciencewares, Falmouth, MA02540, USA) and iFluxes 1.0 (YoungerUSA, LLC, Amherst, MA01002, USA) software [55,56]. The NMT measures ion concentrations using ion-selective microelectrodes in both static and dynamic ways. The absolute concentration of a specific ion or ion concentration gradient was measured by moving the electrode repeatedly between two positions in a predefined excursion (5–30 μm) at a programmable frequency in the range 0.01–10.00 Hz with a range of 0.3–0.5 Hz being typical for many types of electrodes. The ion-selective electrode was constructed as follows: glass micropipettes (2 μm aperture) were pulled from 1.5-mm diameter glass capillaries (TW150-4, World Precision Instruments, Inc., Florida, USA) with an electrode puller (P-97, Sutter Instrument). Pulled micropipettes were silanized with dimethyl-dichlorosilane (D3879, Sigma, St Louis, MO, USA) at 250 °C for 50 min. For all electrodes: an Ag/AgCl wire electrode holder (EHB-1, World Precision Instruments) was inserted in the back of each electrode to create an electrical contact with the electrolyte; the ground reference electrode was an Ag/AgCl half-cell (World Precision Instruments); and only electrodes with Nernstian slopes between 53 and 65 mV were used.

Isolated abaxial peels were soaked in a test bath solution (0.1 mM NaCl, 0.1 mM KCl, 0.15 mM $CaCl_2$, 0.3 mM MES, pH 6.0) for 5 min. The ion-selective electrodes were mounted on a manipulator and positioned 20 μm above a salt gland. A peel in the chamber containing experimental solution was placed on the microscope stage and ion fluxes were measured between 10 μm and 30 μm above the salt gland at intervals of 5.5 s. Net ion fluxes were measured for 15 min for each sample. At least eight samples were measured for each treatment (0 and 200 mM NaCl). Fluxes of Na^+ and K^+ were calculated using MageFlux software developed by Yue Xu (http://www.youngerusa.com/mageflux).

2.10. Statistical analysis

The data were analyzed using SPSS 16.0 (SPSS Inc., Chicago, IL, USA) for Windows and all values reported are the means ± standard deviation (SD). Treatment significance was determined with one-way analyses of variance (ANOVA), and means denoted by different lower-case letters are significantly different at $P < 0.05$ based on Duncan's multiple range test.

3. Results

3.1. Ultrastructure features of L. bicolor salt gland

The use of HPF and FS to fix the leaves was successful and outstanding preservation of salt gland ultrastructure was obtained, as demonstrated by the clearly identifiable intact salt gland in the image shown in Fig. 1. The salt gland of *L. bicolor* consists of sixteen cells, including four outer cup cells (oc), four inner cup cells (ic), four accessory cells (ac), and four secretory cells (sc) (Fig. 1A). Nuclei (n), numerous mitochondria (m, Fig. 1C), small vesicles (v), Golgi (g), rough endoplasmic reticulum (rer), outer surface cuticle (c) are clearly identifiable (Fig. 1B), the nuclei, stained with the DNA-specific fluorescent dye, DAPI (Fig. 2) in these cells are typically large with very prominent nucleoli (nu) (Fig. 1A). A plasmodesma (pl) in a wall between two secretory cells (Fig. 1D) is also clearly visible.

3.2. NaCl treatment enhanced K^+ accumulation in the cytoplasm and nucleus of the salt gland cells

The NanoSIMS ion maps show a cross section of a leaf with the salt-gland complex, and the image resolution is sufficiently high to reveal organelles (Fig. 3). The position of the salt gland for NanoSIMS analysis is shown in Fig. 3A. The SE image showed the integrity and morphology of the sample surface (Fig. 3B). The O^- ion signal (aqua) was particularly strong in the cell walls of the salt gland cells, especially in the adjacent cells (Fig. 3C), the CN^- ion signal (lawngreen) was high specifically in the cytoplasm, notably in the collecting cells, but also the nucleus and nucleolus had a strongly elevated CN^- signal intensity (Fig. 3D). In contrast to the low K^+ signal (aquamarine) in both cytoplasm and nucleus of control (0 mM NaCl, Fig. 3E), clear evidence for markedly elevated K^+ signal (orange) in both cytoplasm and nucleus of NaCl-treated (200 mM NaCl) salt gland cells is shown in Fig. 3F, specifically in the nucleus. The relative signal strength of K^+ in the cytoplasm and nucleus of NaCl-treated salt gland cells was 16.5 and 21.9 times control, respectively (Fig. 4A). The Na^+ signal was specifically high in the intercellular space of both control (Fig. 3G, yellow) and NaCl-treated salt gland cells (Fig. 3H, aqua). Similarly, the relative

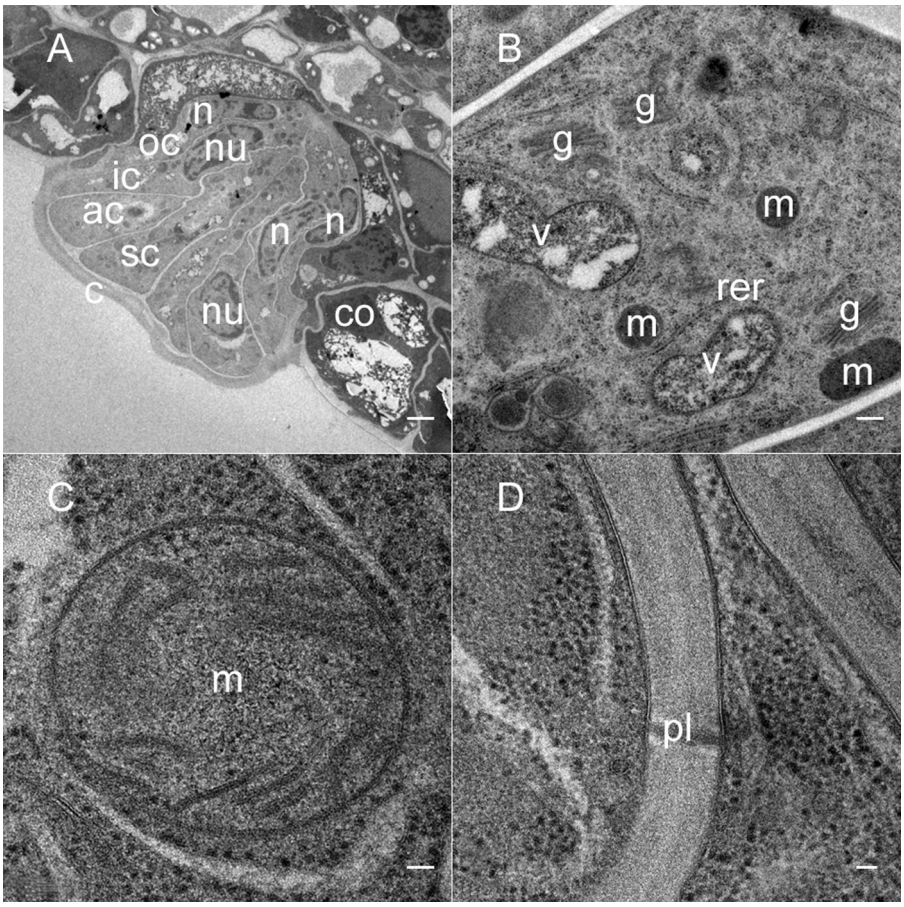

Fig. 1. TEM image of salt gland of *L. bicolor* leaf prepared by HPF, followed by FS and then embedding, sectioning and staining. (A) General view of salt gland of the NaCl-challenged leaf of *L. bicolor*. Outer cup cell (oc), inner cup cell (ic), accessory cell (ac), secretory cell (sc), and collecting cell (co) are noted, c = cuticle, n = nucleus, nu = nucleolus. (B) a high magnification view of the salt gland. g = Golgi, m = mitochondrion, rer = rough endoplasmic reticulum, v = vesicle. (C) enlarged mitochondrion in the secretory cell. m = mitochondrion. (D) plasmodesma in a wall between two secretory cells. pl = plasmodesma. Bars = 2.5 μm (A), 250 nm (B), 50 nm (C, D).

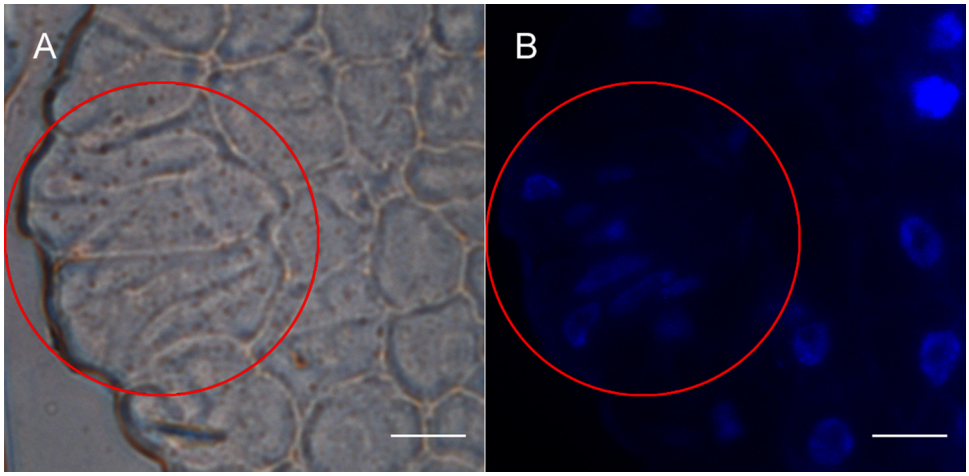

Fig. 2. A cross-section of *L. bicolor* leaf was stained with DAPI and visualized under a bright field (BF, A) and also by the laser scanning confocal microscope (LSCM, B). Red circle indicates salt gland and blue parts are nuclei. Bars = 10 μm. (For interpretation of the references to color in this figure legend, the reader is referred to the web version of this article.)

signal strength of Na^+ in the cytoplasm and nucleus of NaCl-treated salt gland cells was 24.5 and 26.1 times control, but there was no significant difference between the cytoplasm and nucleus of both control and NaCl-treated salt gland cells (Fig. 4B). Interestingly, the K^+/Na^+ ratio was much higher in the nucleus of both control and NaCl-treated salt gland cells than in the cytoplasm, but in this circumstance, K^+/Na^+ ratio in the cytoplasm and nucleus of salt gland cells was slightly reduced by NaCl treatment (Fig. 4C). In control plants, K^+ was the predominant cation at 0 mM NaCl, but its concentration decreased with increasing NaCl concentration to 200 mM

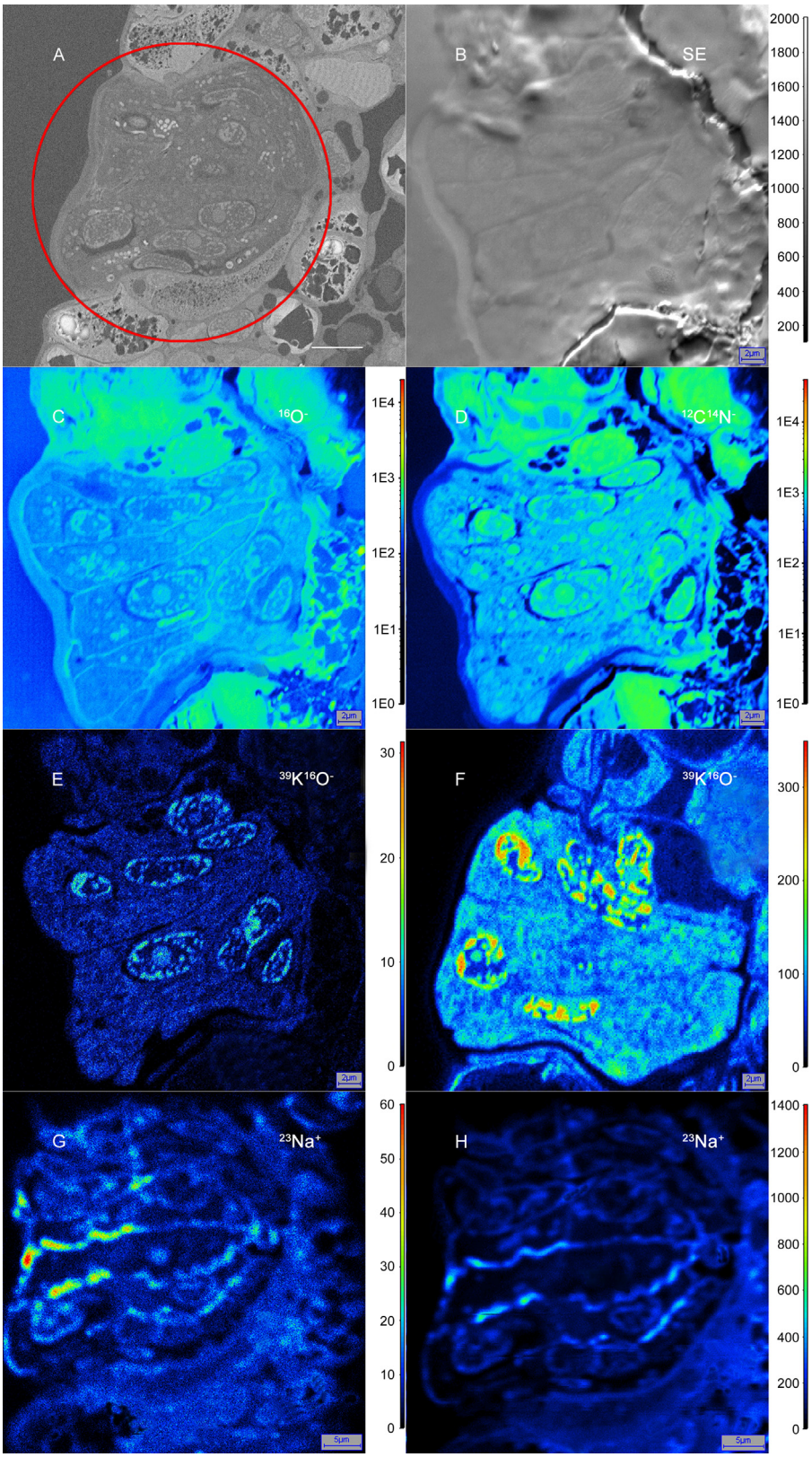

Fig. 3. NanoSIMS analysis of a cross-section of *L. bicolor* leaf prepared by HPF followed by FS. SEM image showed the position of the salt gland for NanoSIMS analysis (A), red circle indicates the salt gland, bar = 5 μm. NanoSIMS maps obtained using the Cs^+ primary ion beam, showing $^{16}O^-$ (C), $^{12}C^{14}N^-$ (D), and $^{39}K^{16}O^-$ (E: 0 mM NaCl; F: 200 mM NaCl) ion maps, the O^- primary ion beam for the distribution of $^{23}Na^+$ (G: 0 mM NaCl; H: 200 mM NaCl) signal, the SE image is included to show the morphology of the imaged region (B). the ordinate scales represents ion signal strength and the brighter the color, the higher the strength. (For interpretation of the references to color in this figure legend, the reader is referred to the web version of this article.)

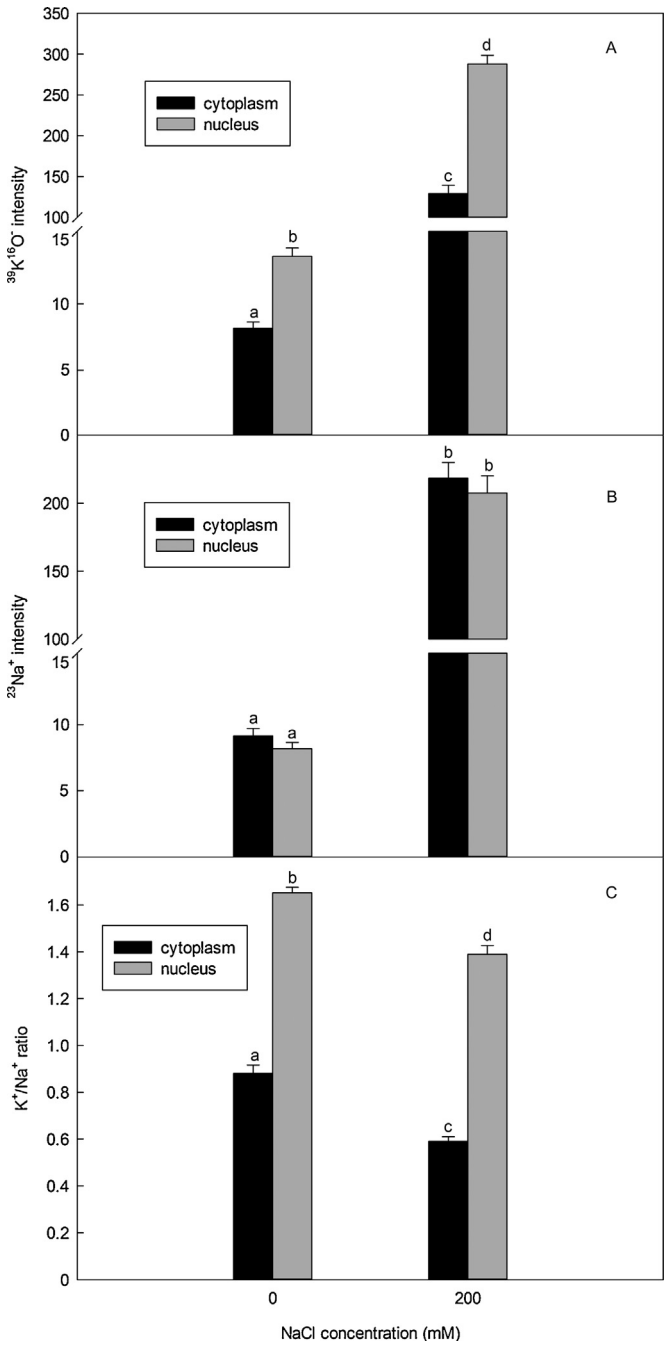

Fig. 4. NanoSIMS composition profiles of a single salt gland of *L. bicolor* for the $^{39}K^{16}O^-$ and $^{23}Na^+$ maps shown in Fig. 3(E–H). (A) shows that the $^{39}K^{16}O^-$ signal originated from different locations in the salt gland. (B) shows that the $^{23}Na^+$ signal originated from different locations in the salt gland. K^+/Na^+ ratio was calculated as shown in (C). Values are means ± SD ($n = 5$). Values followed by the different lower-case letters are significantly different at $P < 0.05$ as determined by Duncan's multiple range test.

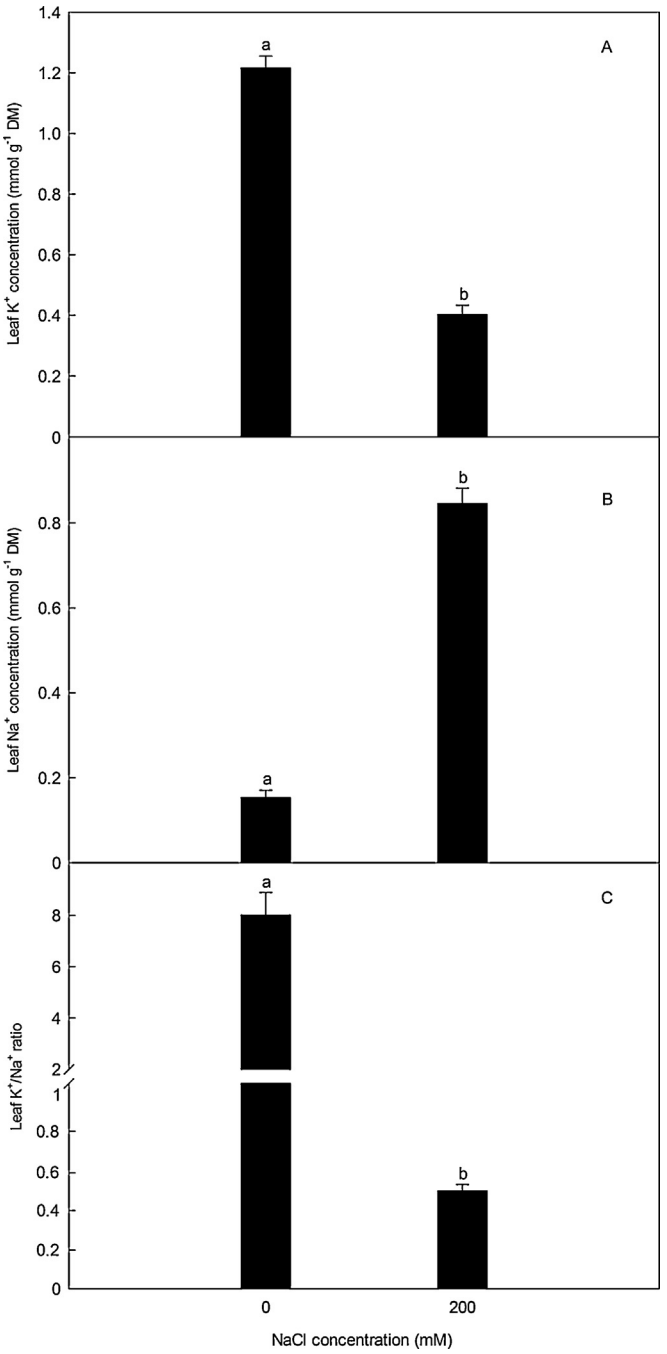

Fig. 5. Leaf K^+ (A) and Na^+ (B) concentrations of *L. bicolor* seedlings treated with 0, and 200 mM NaCl for 28 d. K^+/Na^+ ratio was calculated as shown in (C). Values, which are means ($n = 5$) ± SD, indicate the change in the indicated variables. Values followed by the different lower-case letters are significantly different at $P < 0.05$ according to Duncan's multiple range test.

NaCl (Fig. 5A). However, the leaf Na^+ concentration increased with increasing salinity (Fig. 5B) and the K^+/Na^+ ratio in the leaf tissue was also reduced by 200 mM NaCl treatment (Fig. 5C).

3.3. NaCl treatment markedly increased Na^+ secretion rate but decreased K^+ secretion rate of the salt gland

To look into the possible role of K^+ and Na^+ accumulation in salt secretion by the salt glands, K^+ and Na^+ secretion rates per salt gland were estimated using leaf discs. As shown in Fig. 6, the Na^+ secretion rate from disc treated with 200 mM NaCl was 5.4 times higher than that of control, but K^+ secretion rate was only 30% of control. Similarly, NMT was used to measure directly ion secretion rate of salt glands; again, the secretion rate of Na^+ was greatly enhanced by a 200 mM NaCl treatment, but K^+ secretion rate decreased (Fig. 7).

4. Discussion

Biological application of the latest generation of high-resolution imaging by the SIMS instrumentation opens up the potential to map visually the localization and spatial distribution of important

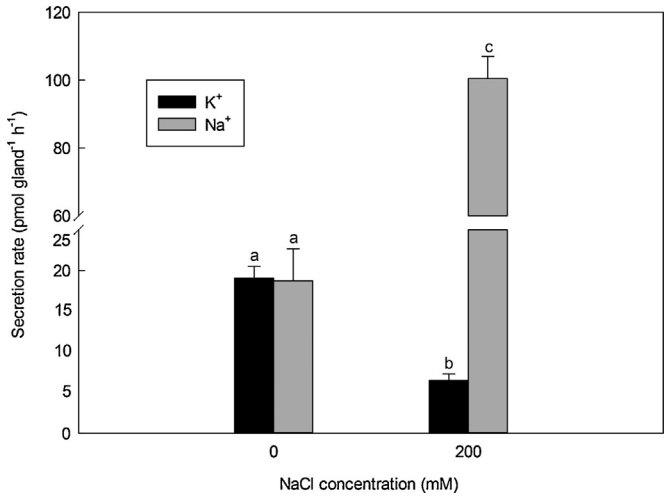

Fig. 6. Ion secretion rates from salt glands of *L. bicolor* leaf discs treated with different concentrations of NaCl (0 and 200 mM). Values, which are means ($n = 5$) ± SD, indicate the change in the indicated variables. Values followed by the different lower-case letters are significantly different at $P < 0.05$ according to Duncan's multiple range test.

chemical elements at the subcellular level with excellent sensitivity and high spatial resolution [32]. Without question, sample preparation is the most critical step in successful NanoSIMS analysis of biological samples, and achievement of the full application of this technique in biology depends primarily on the ability of sample preparation methodologies to preserve the original distribution of elements *in situ* while removing water from the sample [22]. The CN^- ion can be used in the SIMS analysis of biological materials as a marker for the distribution of *N* in nucleic acids and proteins, which permits the visualization of the morphology of the sample, whereas O^- ions are generated preferentially from structures such as cell walls rich in cellulose. In combination, these signals should have the potential to provide information on the ultrastructural localization of important elements in biological samples at high spatial resolution [22]. By scanning a focused primary ion beam across the sample and collecting the secondary ions, the intensities of the component-specific secondary ions detected at each position can be used to construct a map of the sample's surface composition. In the present study, HPF of the leaf samples followed by FS in the acetone substitution medium was found to provide outstanding preservation of salt gland ultrastructure. The mitochondrial cristaes were clearly visible and biomembrane preservation is particularly good (Fig. 1C). As shown in Fig. 1A, cells of the salt gland were much better preserved in our samples for TEM observation using HPF/FS than in those prepared for study using a classical chemical fixation protocol at ambient temperature [27,57]. These results clearly demonstrate that the combination use of HPF and FS can provide superior detail of ultrastructure. HPF/FS is also the proper protocol for the preparation of salt glands for NanoSIMS analysis.

Potassium is an essential macronutrient for living cells and a lack of K^+ significantly reduces plant growth and development [58] and K^+ plays a pivotal role in fundamental physiological processes in

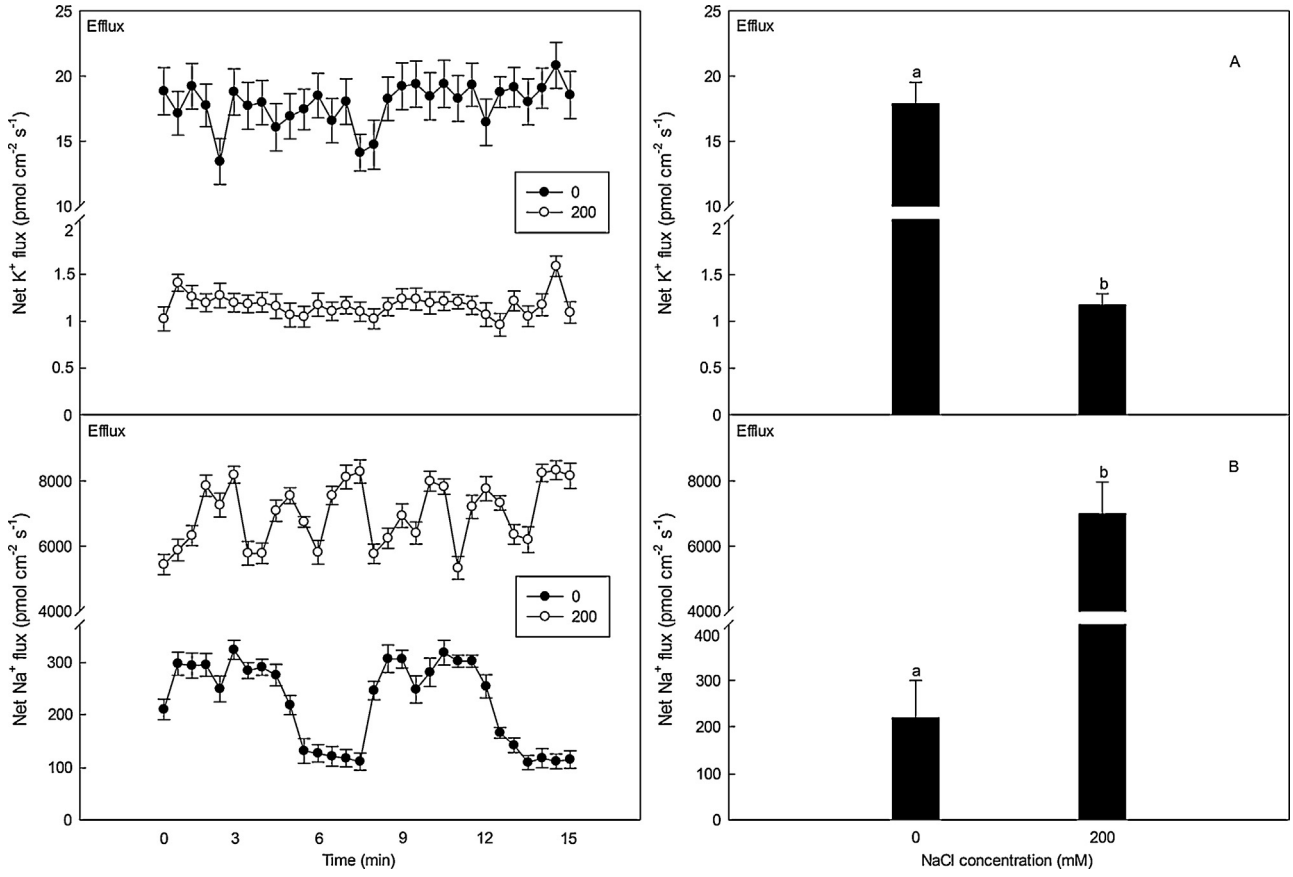

Fig. 7. Effects of different NaCl treatments (0 and 200 mM) on the K^+ (A) and Na^+ (B) secretion rates of salt glands in the abaxial leaf epidermis of *L. bicolor*. Net ion fluxes of K^+ and Na^+ (left hand panels) were measured over 15 min between 10 and 30 μm above each salt gland at intervals of 5.5 s. Each point represents the mean of nine individual salt glands. The right hand panels were the mean fluxes of K^+ and Na^+ with bars representing the standard deviation of the means. Values followed by different lower-case letters are significantly different at $P < 0.05$ as determined by Duncan's multiple range test. Control plants were treated with Hoagland nutrient solution (0 mM NaCl) for 28 d; other plants were treated with Hoagland nutrient solution containing 200 mM NaCl for 28 d.

plants [9,59]. K^+ also plays a role in alleviating the adverse effects of salt stress on growth and enhancing the salinity tolerance of plants, for which maintenance of K^+/Na^+ homeostasis under salinity is an important diagnostic character [1]. In general, K^+ concentration in plant cells is much reduced under saline conditions but Na^+ concentration much increased. Plants can remove excess Na^+ through Na^+ excretion to the external environment and/or compartmentalization into the vacuoles, along with retention of a physiological K^+ concentration in the cytoplasm [60]. Surprisingly, results in the present paper clearly indicate that salt-treated (200 mM NaCl) *L. bicolor* salt gland cells accumulated higher amounts of K^+ than in those of control (0 mM NaCl) plants; in particular, K^+ in the nuclei was much higher than that in the cytoplasm both in salt-treated and control salt gland cells (Fig. 3E,F). Relative signal strength of K^+ in the cytoplasm and nucleus of NaCl-treated salt gland cells was 16.5 and 21.9 times of control, respectively (Fig. 4A). The accumulation of K^+ in the cytoplasm and nucleus may be a contributory factor to salinity tolerance although the exact mechanism between higher K^+ concentration and salinity tolerance is not known. The cytoplasm and nucleus are the centre of metabolic activities such as protein biosynthesis, gene selective expression and regulation [61]. K^+ plays an important role in the activation of the function of enzymes and balances the negative charges on proteins and nucleic acids [62]. Salt secretion of the salt gland is an active physiological process depending on gene expression, protein synthesis, and ATP formation in response to salinity stress [12]. Taken together, we suppose that K^+ accumulation in the cytoplasm and nucleus of NaCl-treated salt gland cells may enhance or stabilize macromolecule synthesis such as proteins and nucleic acids in order to secrete excess salts out of plant cells under salt stress, which is essential for salt secretion, because salt secretion is an energy-dependent process. When grown under salinity, these plants are 'stressed' and K appears to substitute for Na in the salt-secretion mechanism.

High concentration of cytosolic Na^+ is toxic to glycophytes, it disturbs and inhibits various physiological processes and plant growth [7]. The relative signal strength of Na^+ in the cytoplasm and nucleus of NaCl-treated salt gland cells was 24.5 and 26.1 times of control (0 mM NaCl), but there was no significant difference between cytoplasm and nucleus of both control and NaCl-treated salt gland cells (Fig. 4B). However, when *L. bicolor* was treated with 200 mM NaCl, high Na^+ in the cytoplasm and nucleus did not produce harmful effect on salt gland cells, as Na^+ secretion rate of the salt gland treated with 200 mM NaCl was about 5.4 times higher than that of control though K^+ secretion rate was reduced (Fig. 6). NMT results also indicated that secretion rate of Na^+ was greatly enhanced by a 200 mM NaCl treatment, but K^+ secretion rate decreased (Fig. 7). This is consistent with the result that a new analysis of existing data carried out by Colmer et al. [63] suggests that cytosolic Na in halophytes has an activity of 100–200 mM.

The Na^+ signal was specifically high in the intercellular space of both control (Fig. 3G) and NaCl-treated salt gland cells (Fig. 3H) compared to the symplast. The salt gland is encapsulated by a thick cuticular layer (c) except along the region of the walls between the collecting cells (co) and the outer cup cells (Fig. 1A). This non-cuticularized wall region is termed the transfusion area, where ions move from mesophyll cells to the salt gland cells. The major portion of the transpiration water moves from the apoplast to the symplast at the vein endings, so it is probable that the salts, like the water, enter the symplast at the vein endings, then are transported through plasmodesmata (Fig. 1D). The thick cuticle extended over the secretory cells creating a cavity between the cuticular layer and the cell wall of the secretory cells. If salts are transported into the collecting chamber, resulting in the osmotic flow of water into the chamber, osmotic equilibrium within the tissue could be reached before a sufficient hydrostatic pressure develops to force the salty fluid to be secreted through the secretory pores of the salt gland within the cuticle. This indicates that there may be both an apoplastic and a symplastic pathway in the secretion of Na^+ to the outer surface of the leaf of *L. bicolor* [12,13,64,65]. Na^+ accumulation in the apoplast of salt gland cells resulted from enhanced Na^+ secretion (Figs. 6 and 7B).

The capacity of plants to maintain a high cytosolic K^+/Na^+ ratio is likely to be one of the key determinants of plant salt tolerance [66]. In order to improve the K^+/Na^+ ratio under salinity, plants respond promptly to the increased concentrations of Na^+ by maintaining low cytosolic Na^+ and high cytosolic K^+ in the cells [9]. Here, we have shown that the K^+/Na^+ ratio kept a high level, especially in the nucleus when treated with 200 mM NaCl (Fig. 4C), which suggests that high K^+/Na^+ ratio and accumulation of K^+ in the salt gland cells highly correlate with enhanced salt secretion rate and salt tolerance. We also showed that K^+ accumulates higher in the cytoplasm and nucleus of salt-treated salt gland cells than in control, which suggests that K^+ plays an important role in salt secretion possibly via regulation of macromolecule synthesis.

Although the NanoSIMS has many clear advantages such as sufficient analytical sensitivity and high spatial resolution to allow the distribution of elements in these HPF/FS specimens to be visually mapped at the subcellular level, the technique does suffer from a number of shortcomings, which can limit its use. One of the main problems is that quantification is very difficult because the yield of secondary ions from each element is different depending on the electron affinity for negative ions and the ionisation potential for positive ions. Topography can also have a distinct effect on the yield of ions from the sample, restriction of NanoSIMS is that so sensitive to topography of the sample that flat microtome specimens are required. Only flat samples are introduced into the instrument so that real compositional variations are observed rather than just topographical variations. SIMS subjects to the strong matrix effects, and hence signals from the matrix as heterogeneous as plant materials will be detected simultaneously. Biological materials suffer from matrix effects because there can be large variations in the chemistry and structure of the sample in different cells. In general, it has been found that the matrix effects in resin-embedded sample are minimal [67]. Furthermore, TEM analysis determines the correct interpretation of the histological features for the NanoSIMS chemical maps, so the structural preservation of the sample is very crucial. Another concern is the methods used to preserve the specimens prior to analysis. The HPF/FS technique applied here (quick freezing and slow substitution of vitreous ice with chemical fixative) helps to minimize the redistribution of soluble cellular components, but the extent of possible elemental redistribution during sample preparation is an important factor in the preparation of biological specimens for chemical analysis, so the preservation *in situ* testifies to the effectiveness of the HPF/FS protocol in preserving the distribution of soluble elements.

Acknowledgements

We thank professor Sodmergen (Key Laboratory of Ministry of Education for Cell Proliferation and Differentiation, College of Life Sciences, Peking University, Haidian 100871, China) for his technical assistance in fluorescence microscopy. This work was supported by the NSFC [National Natural Science Research Foundation of China, project No. 30870138 and No. 31070158], key projects in the National Science and Technology Pillar program during the eleventh five-year plan period [2009BADA7B05], and Programs Foundation of Ministry of Education of China [20123704130001] band program for scientific research innovation team in colleges and universities of Shandong province.

References

[1] R. Munns, M. Tester, Mechanisms of salinity tolerance, Annu. Rev. Plant Biol. 59 (2008) 651–681.
[2] M.M. Azooz, M.A. Shaddad, A.A. Abdel-Latef, Leaf growth and K^+/Na^+ ratio as an indication of the salt tolerance of three sorghum cultivars grown under salinity stress and IAA treatment, Acta Agron. Hung. 52 (2004) 287–296.
[3] F. Hauser, T. Horie, A conserved primary salt tolerance mechanism mediated by HKT transporters: a mechanism for sodium exclusion and maintenance of high K^+/Na^+ ratio in leaves during salinity stress, Plant Cell Environ. 33 (2010) 552–565.
[4] E. Tavakkoli, F. Fatehi, S. Coventry, P. Rengasamy, G.K. McDonald, Additive effects of Na^+ and Cl^- ions on barley growth under salinity stress, J. Exp. Bot. 62 (2011) 2189–2203.
[5] Y.H. Peng, Y.F. Zhu, Y.Q. Mao, S.M. Wang, W.A. Su, Z.C. Tang, Alkali grass resists salt stress through high [K^+] and an endodermis barrier to Na^+, J. Exp. Bot. 55 (2004) 939–949.
[6] R.A. James, R. Munns, S. von Caemmerer, C. Trejo, C. Miller, T. Condon, Photosynthetic capacity is related to the cellular and subcellular partitioning of Na^+, K^+ and Cl^- in salt-affected barley and durum wheat, Plant Cell Environ. 29 (2006) 2185–2197.
[7] F.J.M. Maathuis, A. Amtmann, K^+ nutrition and Na^+ toxicity: the basis of cellular K^+/Na^+ ratios, Ann. Bot. 84 (1999) 123–133.
[8] J.M. Pardo, B. Cubero, E.O. Leidi, F.J. Quintero, Alkali cation exchangers: roles in cellular homoestasis and stress tolerance, J. Exp. Bot. 57 (2006) 1181–1199.
[9] E. Adams, R. Shin, Transport, signalling, and homeostasis of potassium and sodium in plants, J. Integr. Plant Biol. 56 (2014) 231–249.
[10] S.W. Breckle, How do Halophytes Overcome Salinity, in: M.A. Khan, I.A. Ungar (Eds.), Biology of Salt Tolerant Plants, Book Crafters, Michigan, 1995, pp. 199–213.
[11] T.J. Flowers, T.D. Colmer, Salinity tolerance in halophytes, New Phytol. 179 (2008) 945–963.
[12] F. Ding, J.C. Yang, F. Yuan, B.S. Wang, Progress in mechanism of salt excretion in recretohalopytes, Front. Biol. 5 (2010) 164–170.
[13] W.W. Thomson, L.L. Liu, Ultrastructural features of the salt gland of *Tamarix aphylla* L, Planta 73 (1967) 201–220.
[14] C.A. Levering, W.W. Thomson, The ultrastructure of the salt gland of *Spartina foliosa*, Planta 97 (1971) 183–196.
[15] M.A. Fitzgerald, D.A. Orlovich, W.G. Allaway, Evidence that abaxial leaf glands are the sites of salt secretion in leaves of the mangrove *Avicennia marina* (Forsk.) Vierh, New Phytol. 120 (1992) 1–7.
[16] W.H. Arisz, I.J. Camphuis, H. Heikens, A.J. van Tooren, The secretion of the salt glands of *Limonium latifolium* Ktze, Acta Bot. Neerl. 4 (1955) 322–338.
[17] H. Ziegler, U. Lüttge, Die Salzdrüsen von *Limonium vulgare*, Planta 74 (1967) 1–17.
[18] C. Shimony, A. Fahn, Light- and electron-microscopical studies on the structure of salt glands of *Tamarix aphylla* L, J. Linnean Soc. 60 (1968) 283–288.
[19] D.A. Orlovich, A.E. Ashford, X-ray microanalysis of ion distribution in frozen salt/dextran droplets after freeze-substitution and embedding in anhydrous conditions, J. Microsc. 180 (1995) 117–126.
[20] P. Echlin, Biological X-ray microanalysis: the past, present practices, and future prospects, Microsc. Microanal. 7 (2001) 211–219.
[21] J. van Zyl, Q.G. Forrest, C. Hocking, C.K. Pallaghy, Freeze-substitution of plant and animal tissue for the localization of water-soluble compounds by electron probe microanalysis, Micron 7 (1976) 213–224.
[22] K.E. Smart, J.A.C. Smith, M.R. Kilburn, B.G.H. Martin, C. Hawes, C.R.M. Grovenor, High-resolution elemental localization in vacuolate plant cells by nanoscale secondary ion mass spectrometry, Plant J. 63 (2010) 870–879.
[23] S.D. Bidwell, S.A. Crawford, I.E. Woodrow, J. Sommer-Knudsen, A.T. Marshall, Sub-cellular localization of Ni in the hyperaccumulator, *Hybanthus floribundus* (Lindley) F. Muell, Plant Cell Environ. 27 (2004) 705–716.
[24] P. Walther, E. Schmid, K. Höhn, High-pressure freezing for scanning transmission electron tomography analysis of cellular organelles, in: D.J. Taatjes, J. Roth (Eds.), Cell Imaging Techniques: Methods and Protocols, Methods in Molecular Biology, Humana Press, New Jersey, 2013, pp. 525–535.
[25] D. Studer, W. Graber, A. Al-Amoudi, P. Eggli, A new approach for cryofixation by high-pressure freezing, J. Microsc. 203 (2001) 285–294.
[26] D.D. Klug, Glassy water, Science 294 (2001) 2305–2306.
[27] S.P. Li, M. Chen, D.L. Yu, S.C. Ren, S.F. Sun, L.D. Liu, T. Ketelaar, A.M.C. Emons, C.M. Liu, EXO70A1-mediated vesicle trafficking is critical for tracheary element development in *Arabidopsis*, Plant Cell 25 (2013) 1774–1786.
[28] A. Benninghoven, Surface analysis by secondary ion mass spectrometry (SIMS), Surf. Sci. 299-300 (1994) 246–260.
[29] P. Hoppe, S. Cohen, A. Meibom, NanoSIMS: technical aspects and applications in cosmochemistry and biological geochemistry, Geostand. Geoanal. Res. 37 (2013) 111–154.
[30] J. Bougoure, M. Ludwig, M. Brundrett, J. Cliff, P. Clode, M. Kilburn, P. Grierson, High-resolution secondary ion mass spectrometry analysis of carbon dynamics in mycorrhizas formed by an obligately myco-heterotrophic orchid, Plant Cell Environ. 37 (2014) 1223–1230.
[31] M.L. Steinhauser, A.P. Bailey, S.E. Senyo, C. Guillermier, T.S. Perlstein, A.P. Gould, R.T. Lee, C.P. Lechene, Multi-isotope imaging mass spectrometry quantifies stem cell division and metabolism, Nature 481 (2012) 516–519.
[32] H.A. Klitzing, P.K. Weber, M.L. Kraft, Secondary ion mass spectrometry imaging of biological membranes at migh spatial resolution, in: A.A. Sousa, M.J. Kruhlak (Eds.), Nanoimaging: Methods and Protocols, Methods in Molecular Biology, Humana Press, New Jersey, 2013, pp. 483–501.
[33] K.L. Moore, M. Schroder, Z.C. Wu, B.G.H. Martin, C.R. Hawes, S.P. McGrath, M.J. Hawkesford, J.F. Ma, F.J. Zhao, C.R.M. Grovenor, High-resolution secondary ion mass spectrometry reveals the contrasting subcellular distribution of arsenic and silicon in rice roots, Plant Physiol. 156 (2011) 913–924.
[34] K.L. Moore, E. Lombi, F.J. Zhao, C.R.M. Grovenor, Elemental imaging at the nanoscale: nanoSIMS and complementary techniques for element localisation in plants, Anal. Bioanal. Chem. 402 (2012) 3263–3273.
[35] K.H. Lau, M. Christlieb, M. Schröder, H. Sheldon, A.L. Harris, C.R.M. Grovenor, Development of a new bimodal imaging methodology: a combination of fluorescence microscopy and high-resolution secondary ion mass spectrometry, J. Microsc. 240 (2010) 21–31.
[36] F.J. Zhao, K.L. Moore, E. Lombi, Y.G. Zhu, Imaging element distribution and speciation in plant cells, Trends Plant Sci. 19 (2014) 183–192.
[37] M.S. Burns, Applications of secondary ion mass spectrometry (SIMS) in biological research: a review, J. Microsc. 127 (1982) 237–258.
[38] N. Grignon, S. Halpern, J. Jeusset, P. Fragu, Secondary ion mass spectrometry (SIMS) microscopy as an imaging tool for physiological studies II. SIMS microscopy of plant tissues, Microsc. Microanal. 2 (1996) 129–136.
[39] R. Tartivel, R. Tatin, T. Delhaye, A. Maupas, A. Gendron, S. Gautier, O. Lavastre, Visualization and localization of bromotoluene distribution in Hedera helix using NanoSIMS, Chemosphere 89 (2012) 805–809.
[40] K.L. Moore, Y. Chen, A.M.L. van de Meene, L. Hughes, W.J. Liu, T. Geraki, F. Mosselmans, S.P. McGrath, C. Grovenor, F.J. Zhao, Combined NanoSIMS and synchrotron X-ray fluorescence reveal distinct cellular and subcellular distribution patterns of trace elements in rice tissues, New Phytol. 201 (2014) 104–115.
[41] M.R. Kilburn, P.L. Clode, Elemental and isotopic imaging of biological samples using NanoSIMS, in: K. John (Ed.), Electron Microscopy: Methods and Protocols, Methods in Molecular Biology, Humana Press, New Jersey, 2014, pp. 733–755.
[42] T.H. Giddings, Freeze-substitution protocols for improved visualization of membranes in high-pressure frozen samples, J. Microsc. 212 (2003) 53–61.
[43] U. Kramer, I.J. Pickering, R.C. Prince, I. Raskin, D.E. Salt, Subcellular localization and speciation of nickel in hyperaccumulator and non-accumulator *Thlaspi* species, Plant Physiol. 122 (2000) 1343–1354.
[44] A. Saito, M. Saito, Y. Ichikawa, M. Yoshiba, T. Tadano, E. Miwa, K. Higuchi, Difference in the distribution and speciation of cellular nickel between nickel-tolerant and non-tolerant *Nicotiana tabacum* L. cv. BY-2 cells, Plant Cell Environ. 33 (2010) 174–187.
[45] M.A. Morales, E. Olmos, A. Torrecillas, M.J. Sanchez-Blanco, J.J. Alarcon, Differences in water relations, leaf ion accumulation and excretion rates between cultivated and wild species of *Limonium* sp. grown in conditions of saline stress, Flora 196 (2001) 345–352.
[46] Y. Li, Kinetics of the antioxidant response to salinity in the halophyte *Limonium bicolor*, Plant Soil Environ. 54 (2008) 493–497.
[47] Y.C. Wang, H. Ma, G.F. Liu, C.X. Xu, D.W. Zhang, Q.Y. Ban, Analysis of gene expression profile of *Limonium bicolor* under NaHCO3 stress using cDNA microarray, Plant Mol. Biol. Rep. 26 (2008) 241–254.
[48] F. Yuan, M. Chen, B.Y. Leng, B.S. Wang, An efficient autofluorescence method for screening *Limonium bicolor* mutants for abnormal salt gland density and salt secretion, S. Afr. J. Bot. 88 (2013) 110–117.
[49] X.C. Zhao, C. Floss, Y.T. Lin, M. Bose, Stardust investigation into the CR chondrite grove mountain 21,710, Astrophys. J. 769 (2013) 49–64.
[50] N. Nagata, C. Saito, A. Sakai, H. Kuroiwa, T. Kuroiwa, The selective increase or decrease of organellar DNA in generative cells just after pollen mitosis one controls cytoplasmic inheritance, Planta 209 (1999) 53–65.
[51] D.Y. Wang, Q. Zhang, Y. Liu, Z.F. Lin, S.X. Zhang, M.X. Sun, Sodmergen, the levels of male gametic mitochondrial dna are highly regulated in angiosperms with regard to mitochondrial inheritance, Plant Cell 22 (2010) 2402–2416.
[52] C.D. Faraday, P.M. Quinton, W.W. Thomson, Ion fluxes across the transfusion zone of secreting *Limonium* salt glands determined from secretion rates, transfusion zone areas and plasmodesmatal frequencies, J. Exp. Bot. 37 (1986) 482–494.
[53] W.J. Dschida, K.A. Platt-Aloia, W.W. Thomson, Epidermal peels of *Avicennia germinans* (L.) Stearn: a useful system to study the function of salt glands, Ann. Bot. 70 (1992) 501–509.
[54] R.A. Balsamo, M.E. Adams, W.W. Thomson, Electrophysiology of the salt glands of *Avicennia germinans*, Int. J. Plant Sci. 156 (1995) 658–667.
[55] Y.Q. Yang, Y.X. Qin, C.G. Xie, F.Y. Zhao, J.F. Zhao, D.F. Liu, S.Y. Chen, A.T. Fuglsang, M.G. Palmgren, K.S. Schumaker, X.W. Deng, Y. Guo, The *Arabidopsis* chaperone J3 regulates the plasma membrane H^+-ATPase through interaction with the PKS5 kinase, Plant Cell 22 (2010) 1313–1332.
[56] X.Q. Kong, Z. Luo, H.Z. Dong, A.E. Eneji, W.J. Li, Effects of non-uniform root zone salinity on water use Na^+ recirculation, and Na^+ and H^+ flux in cotton, J. Exp. Bot. 63 (2012) 2105–2116.
[57] A.E. Vassilyev, A.A. Stepanova, The ultrastructure of ion-secreting and non-secreting salt glands of *Limonium platphyllum*, J. Exp. Bot. 41 (1990) 41–46.
[58] A. Rodríguez-Navarro, F. Rubio, High-affinity potassium and sodium transport systems in plants, J. Exp. Bot. 57 (2006) 1149–1160.
[59] D. Golldack, F. Quigley, C.B. Michalowski, U.R. Kamasani, H.J. Bohnert, Salinity stress-tolerant and -sensitive rice (*Oryza sativa* L.) regulate AKT1-type potassium channel transcripts differently, Plant Mol. Biol. 51 (2003) 71–81.

[60] R. Olias, Z. Eljakaoui, J. Li, P.A.D. Morales, M.C. Marin-Manzano, J.M. Pardo, A. Belver, The plasma membrane Na^+/H^+ antiporter SOS1 is essential for salt tolerance in tomato and affects the partitioning of Na^+ between plant organs, Plant Cell Environ. 32 (2009) 904–916.
[61] A.I. Lamond, W.C. Earnshaw, Structure and function in the nucleus, Science 280 (1998) 547–553.
[62] M.K. Ashley, M. Grant, A. Grabov, Plant responses to potassium deficiencies: a role for potassium transport proteins, J. Exp. Bot. 57 (2006) 425–436.
[63] T.D. Colmer, T.J. Flowers, R. Munns, Use of wild relatives to improve salt tolerance in wheat, J. Exp. Bot. 57 (2006) 1059–1078.
[64] J. Rozema, H. Gude, F. Bijkf, H. Wesselman, Sodium concentration in xylem sap in relation to ion exclusion, accumulation and secretion in halophytes, Acta Bot. Neerl. 30 (1981) 309–311.
[65] M.A. Fitzgerald, W.G. Allaway, Apoplastic and symplastic pathways in the leaf of the grey mangrove *Avicennia marina* (Forsk.) Vierh, New Phytol. 119 (1991) 217–226.
[66] W.S. Pierce, N. Higinbotham, Compartments and fluxes of K^+, Na^+ and Cl^- in Avena coleoptile cells, Plant Physiol. 46 (1970) 666–673.
[67] J.T. Brenna, G.H. Morrison, Ionization probability variations due to matrix in ion microscopic analysis of plastic-embedded and ashed biological specimens, Anal. Chem. 58 (1986) 1675–1680.